ISSN: 1687-1006 p
ISSN: 2682-3640 c

The Egyptian International Journal of Engineering Sciences and Technology

https://eijest.journals.ekb.eg/

Vol. 49 (2025) 90–99

DOI: 10.21608/EIJEST.2024.283844.1271

Frequency Reconfigurable SIW Antenna for Millimeter-Wave Applications

Samar M. Azab[a]*, Abdelhamid. A. Shaalan[b], Khalid. F. A. Hussein[c], Asmaa E. Farahat[c]

[a]*Zagazig Higher Institute of Engineering & Technology, Zagazig, Egypt*
[b]*Electronics and Comm. Engineering Department, Faculty of Engineering, Zagazig University Zagazig, Egypt*
[c]*Microwave Engineering Department, Electronics Research Institute (ERI), 11843, Cairo, Egypt*

ARTICLE INFO

Article history:

Received 19 April 2024
Received in revised form 29 July 2024
Accepted 29 July 2024
Available online 29 July 2024

Keywords:

Reconfigurable Antenna, Frequency Reconfigurable, Substrate Integrated Waveguide Antenna, Millimeter-Wave Antenna

ABSTRACT

A reconfigurable millimeter-wave (28/38 GHz) antenna is proposed for future generations of mobile communication. The antenna is constructed as dual-slot on substrate integrated waveguide (SIW) cavity. The two slots are parallel and cut in the upper wall of the SIW cavity. This antenna is reconfigurable and canoperate at either 28 or 38 GHz by a rotary strip. This strip can be rotated while touching the external surface of the upper wall of the SIW cavity by means of a micro-electro-mechanical system (MEMS) servomotor. When the rotary strip is rotated to be perpendicular to the axis of symmetry of the antenna and feeding line (i.e. parallel to the slots) it operates at 28 GHz. When the rotary strip is rotated to be aligned with the axis of symmetry (perpendicular to the slots) the antenna operates at 38 GHz. In latter case, each slot is divided into two slots to form four radiating slots of the same length. The dual-slot antenna structure enhances the radiation efficiency at both 28 and 38 GHz. The antenna has impedance matching bandwidths of 1.1GHz and 0.9 GHz about the center frequencies 28 and 38 GHz, respectively. The values of the maximum gain produced at 28 and 38 GHz are 5.4 and 6 dBi, respectively. The corresponding radiation efficiencies are 80.5% and 82%, respectively. For experimental validation of the simulation results, a prototype is fabricated for the proposed antenna. The measurements and simulation results agree well with each other.

1. Introduction

To meet the requirements for the present and future generations of wireless communication, modern antennas should be designed to enhance the performance of communication system under variable operational and environmental conditions. In practical applications, the RF environment is continuously changing leading to face real-time problems that result in signal distortion and thereby degrades the communication system performance. Overcoming multipath, interference and fading in such continuously varying conditions are some of the challenges that face the communication system designer. Reconfigurable antennas have the ability to adapt themselves to the continuously varying conditions in RF environment. Such antennas can be frequency, pattern, and polarization reconfigurable and should respond in real time. Frequency

* Corresponding author. Tel.: +201098069731
E-mail address: samar.omar5555@gmail.com

reconfigurable antennas may be able to switch from one resonant frequency to another, change the bandwidth, and adding notches (narrow stop bands) in a wide frequency band [1, 2]. Pattern reconfigurable antenna may be able to switch between radiation patterns of different shapes and perform beam switching and null steering [3, 4]. Polarization reconfigurable antennas may be able to switch among different polarizations including vertical, horizontal, and circular polarizations of varying sense [5, 6].

The switching elements used for electrical or optical control of reconfigurable antennas include RF switches based on micro-electro-mechanical systems (MEMS), p-intrinsic-n (PIN) junction diodes, varactor diodes, field-effect-transistors (FETs), and photoconductors [7-9]. RF MEMS uses electrically controlled mechanical movements generated by micro- or nano-actuators to perform RF switching in antenna and transmission line elements. GaAs PIN Diodes are used as electronically controlled high speed RF switches. Varactors are p-n junction diodes with electrically controllable capacitance. FETs are fabricated by GaAS technology to be used as high-frequency RF switches. Varactors are usually used for applications requiring continuously tunable frequency. Photoconductors are optical-based switches that are controlled by optical signal of the appropriate wavelength.

Recently, numerous research efforts have been conducted with remarkable contributions to the field of reconfigurable antenna design. In [10], a frequency reconfigurable SIW rectangular-ring slot antenna is proposed. PIN diode switches are used to configure the antenna operation in the S and C bands of the microwave spectrum. In [11], a frequency reconfigurable SIW is proposed to select the operating frequency within the range 4.5 to 12.5 GHz. RF MEMS switch is used to configure the frequency by changing the antenna size using a rectangular patch and U-shaped patch. In [5], a polarization reconfigurable SIW antenna array is proposed to operate in the sub-six GHz band. PIN switches are used to set the polarization of the antenna as left-hand circular polarization (LHCP), right-hand circular polarization (RHCP), or linear polarization (LP).

In [3], a pattern reconfigurable millimeter-wave antenna is proposed to operate at 35 GHz. The antenna is constructed of main patch, two secondary patches, and two parasitic elements. The shape of the radiation pattern can be selected by two RF MEMS switches. In [12], a frequency reconfigurable millimeter-wave SIW antenna is proposed. The frequency of operation can be tuned between 28 and 38 GHz. is performed by two PIN diode switches as the switching element. In [13], a frequency reconfigurable millimeter-wave SIW antenna is proposed. This antenna can be configured by means of two PIN diodes to operate at either 28 or 38 GHz. In [14], a frequency reconfigurable millimeter-wave L-slot antenna is proposed to operate at 42.36, 47.65, 53.13, and 56.72 GHz. The frequency selection is achieved by means of two RF MEMS switches. In [1], a frequency reconfigurable 16-element antenna array of printed elements is proposed to produce circular polarization for millimeter-wave applications at 25, 26, 27.75 and 29 GHz. The frequency of operation is selected using two PIN diodes.

PIN diodes, FET switches, varactors, microfluidics and liquid crystals act well at microwave and lower millimeter-wave frequencies (below 90 GHz). At frequencies higher than 90 GHz, the performance of these switches is dramatically degraded. RF switches driven by MEMS actuators give higher performance when used for reconfigurable antennas operating at higher millimeter-wave frequencies [7]. MEMS actuators use mechanical movement to achieve a short or open circuit configuration through electrostatic force. When used for reconfigurable millimeter-wave antennas, MEMS actuators are characterized by perfect linearity [4] very high isolation, low insertion loss (0.05 – 0.2 dB), very low power consumption (0.05 – 0.1 mW), and almost zero biasing current [2].

In this work, a MEMS actuator based frequency reconfigurable millimeter-wave antenna is proposed. The antenna is constructed as dual-slot on SIW cavity. The two slots are parallel and cut in the upper wall of the SIW cavity. This antenna can be reconfigured to operate at either 28 or 38 GHz by a rotary strip. This strip can be rotated while touching the external surface of the upper wall of the SIW cavity by means of a MEMS actuator. The proposed antenna can be regarded as comprised of three main elements, the resonant SIW cavity, the radiating slots on the upper wall of the cavity, and the configuring strip with the MEMS actuator.

The 28/38 GHz system can be used in many applications like, the high speed mobile networks, entertainment and multimedia, satellite internet, and internet of things in smart homes, smart cities, health care and mission-critical applications, drone operation, and automotive.

The remaining of the present paper is organized as follows. Section 2 presents a detailed description of the SIW antenna design. Section 3, provides some examples of the parametric study performed to get

the optimum dimensions of the proposed SIW antenna. Section 4 presents the simulation results related to the antenna performance with elaborate discussions. Section 5 is concerned with the description of the antenna fabrication and the experimental work. Section 6 presents comparisons with other antenna designs introduced in recent publications. Finally, Section 7 is concerned with the conclusions of the present work.

2. Antenna Design

The proposed antenna can be regarded as comprised of three main elements, the resonant SIW cavity, the radiating slots on the upper wall of the cavity, and the configuring strip with the MEMS actuator.

2.1. Design of the SIW Cavity

The upper and lower faces of the rectangular cavity are formed by the metallic coats on the two faces of the substrate. The left and right walls of the cavity are formed by six vias, whereas the front wall is formed by eight vias. The back wall of the cavity is formed by six vias, where a gap is left at the centre of this wall to allow feeding the cavity with a microstrip time as shown in Figure 1. The vias are uniformly distributed along the circumference of the cavity. The dimensions of the cavity are presented in Figure 1. The diameter of the vias is D_v and the distance between contiguous vias (from center to center) is D_L.The outer dimensions of the upper and lower boundaries of the cavity are $L_P \times W_P$.The dimensions of the rectangular cavity are $L \times W$ (measured from center to center of the vias). The height of the cavity is$h$, which the thickness of the substrate is.
A microstrip line with inset feed is used for feeding the antenna, where the inset length isL_I. The width of the slits on the sides of the inset feed isW_I. The width of the microstrip line feeder is $W_F$and its length isL_F. As shown in Figure 2, the region of the microstrip line (at the feed point) is tapered to help impedance matching and allow the correct contact with the coaxial launcher inner conductor for measurement. The dimensions of the substrate and ground plane are$L_S \times W_P$, where$L_S = L_P + L_F$.

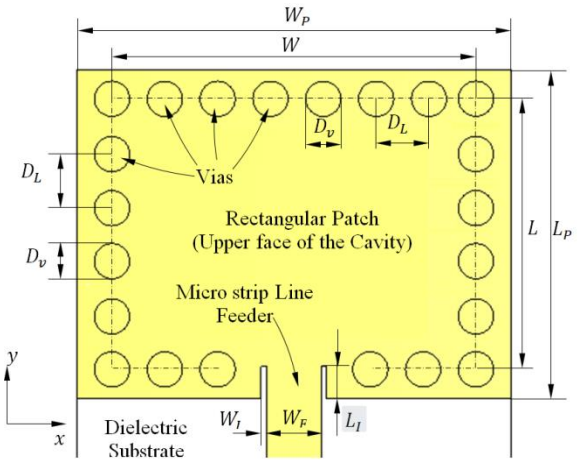

Fig.1: Geometry of the SIW cavity fed with microstrip line

2.2. Design of the Radiating Slot and Rotary Strip

Two parallel radiating slots are cut in the upper face of the cavity as shown in Figure 2a. Each slot has a width S_R and Length L_R.The distance between the radiating slots is D_R. The two slots are positioned symmetrically around the center point of the upper wall of the cavity. A rotary strip of length L_R and width $W_R$is mounted on the external face of the upper wallof the SIWcavity. This strip can be rotated about its center by angle Ψ using a MEMS actuator, which acts as a servo-motor whose axis of rotation coincides with the centerof the upper wall of the cavity. In this way, the angle Ψcan be electrically controlled to configure the dual-slot antenna. When$\Psi = 0°$, the antenna is dual-slot radiator with identical slots. At this orientation of the rotary strip, see Figure 2b, the antenna operates at 28 GHz. When$\Psi = 90°$, the antenna has four radiating slots each of nearly $L_R/2$ length as shown in Figure 2c.

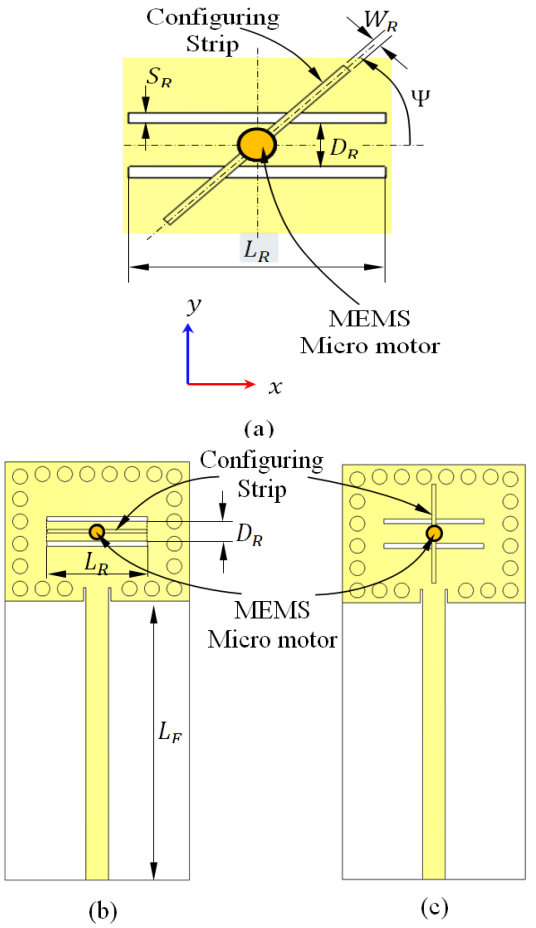

Fig.2: The geometry of the proposed reconfigurable dual-slot SIW antenna. (a) The angle $\Psi_R$of the rotary strip selects the frequency. (a) The two slots and the configuring strip. (a) $\Psi = 0°$ for operation at 28 GHz. (b) $\Psi = 90°$ for operation at 38 GHz.

2.3. MEMS Actuator for Antenna Configuration

The micro-electro-mechanical system (MEMS) motor shown in Figure 3 is an example of semiconductor fabrication technology that have been established many years ago to produce micro-mechanical actuators [15-17].The rotor of this micromotor has diameter of 120 microns. Its principle of operation depends on electrostatic force (not magnetic force) between the poles of the stator and rotor. Owing to the very small dimensions, a very low voltage difference between the poles (few volts) can be enough to build up very high electric fields. Such micromotors are not constructed using discrete components. The tiny parts of such electromechanical system are etched/and or deposited on asemiconductor substrate with post processing procedure to allow the rotation of the structural layers. Such type of micromotors can be integrated with the required driving CMOS circuitry by means of monolithography, in one semiconductor chip. In the proposed reconfigurable SIW antenna, this type of micromotors can be integrated on the upper surface of the top wall of the SIW cavity with its axis coincident with the center point of this wall.

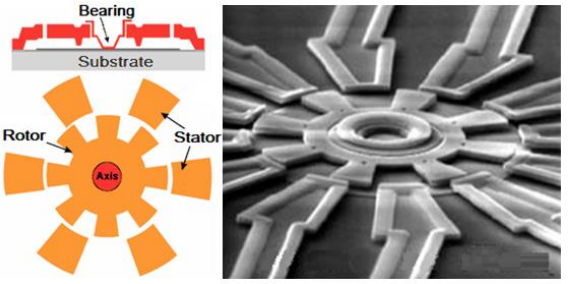

Fig. 3: Integrated electrostatic MEMS micro-motor. The diameter of the rotor is **120 µm** [15-17].

2.4. Optimum Dimensions

The values of the design parameters indicated in Figures 1 and 2 are determined by complete parametric study in order to achieve impedance matching at 28 GHz when $\Psi = 0°$ and 38 GHz when $\Psi = 90°$ with the maximum possible bandwidths. Some examples of the parametric study are presented in Section 3. The optimum dimensions of the propose antenna to achieve the design goals mentioned above are listed in Table 1.

Table 1: Dimensions of the dual-slot SIW antenna whose geometry is shown in Figures 2 and 3.

Parameter	W	L	D_v	D_L	L_F	W_F	W_P	L_P
Value (mm)	6.2	4.5	0.6	0.9	11.2	0.92	7.4	5.6
Parameter	L_R	D_R	W_R	L_I	W_I			
Value (mm)	4.03	1.0	0.15	0.55	0.1			

3. Parametric Study for Optimum Antenna Design

In this section, some examples of the effects of changing the design parameters on the impedance matching bandwidth are presented and discussed. The purpose of this presentation is to explain how the optimum values of the design parameters can be obtained to arrive at the best design of the reconfigurable SIW antenna proposed in the present work.

3.1. Effect of the Slot Length

Changing the length L_R of the radiating slots has significant effects on the frequency response of $|S_{11}|$ as shown in Figure 4. The locations of resonance (sharp minima of $|S_{11}|$) when the antenna is configured to operate at 28 GHz as well 38 GHz ($\Psi = 90°$) are sensitive to that changes of L_R. It is shown that the value of $L_R = 4.03$ mmresults in that the first resonance occurs exactly at 28 GHz for $\Psi = 0°$, whereas the second resonance occurs exactly at 38 GHz for $\Psi = 90°$.

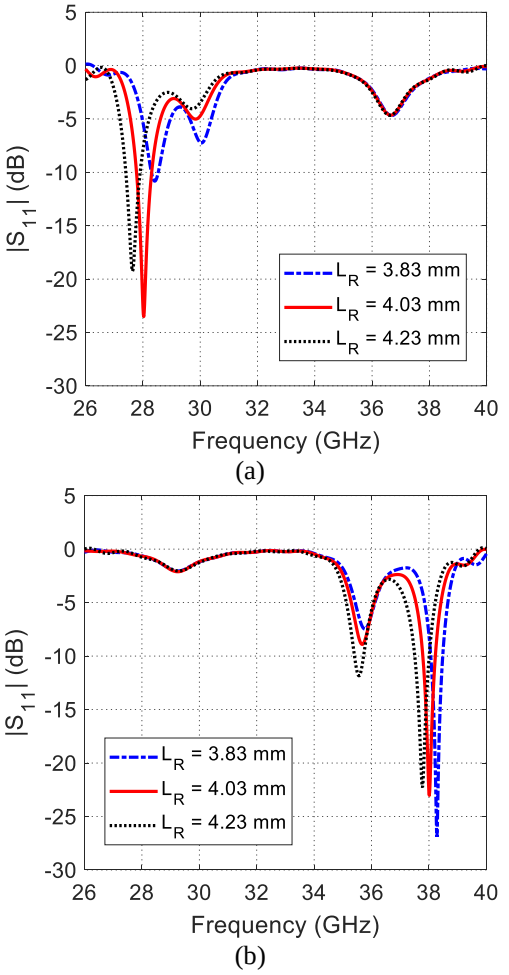

Fig. 4: Effect of changing the slot length, L_R, on the frequency response of $|S_{11}|$ for (a) $\Psi = 0°$ and (b) $\Psi = 90°$.

3.2. Effect of the Distance between the Slots

The effects of changing the distance, D_R, between the two slots on the frequency response of $|S_{11}|$ when the antenna is configured to operate at 28 GHz ($\Psi = 0°$)as well as 38 GHz ($\Psi = 90°$) are presented in Figure 5. It is shown that the value of D_R has a significant effect on the location of resonance (the frequency of anti-peak of$|S_{11}|$) at the two frequency bands. It is clear that setting $D_R = 1.0$ mm results in that the two resonances (obtained with different configurations) occur exactly at 28 and 38 GHz.

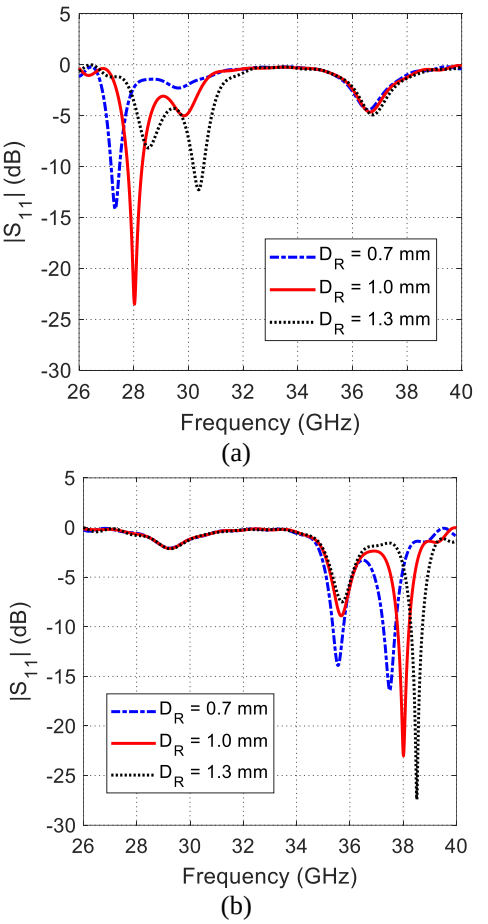

Fig. 5: Effect of changing the distance, D_R, between the slots on the frequency response of $|S_{11}|$ for (a) $\Psi = 0°$ and (b) $\Psi = 90°$.

3.3. Effect of the Inset Length

The inset feed using the microstrip line feeder helps to improve the antenna impedance matching at the desired frequencies. The effects of changing the inset length, L_I, on the frequency response of $|S_{11}|$ when the antenna is configured to operate at 28 GHz as well as 38 GHz are presented in Figure 6. It is shown that the value of L_I has a significant effect on the location of resonance at the first frequency band (28 GHz). However, the location of resonance at the other frequency (38 GHz) is almost unaffected by changing L_I. It is shown that the two resonances (configured by setting $\Psi = 0°$ and $\Psi = 90°$) occur exactly at 28 and 38 GHz when $L_I = 0.55$ mm.

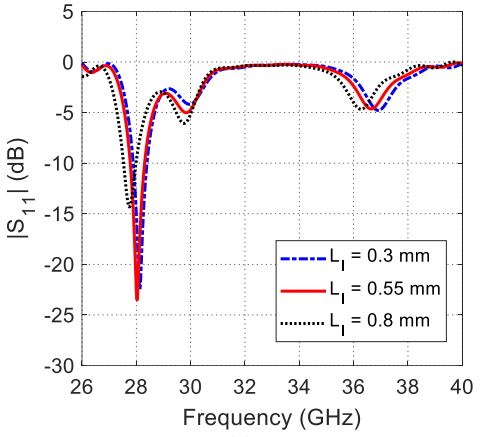

(a)

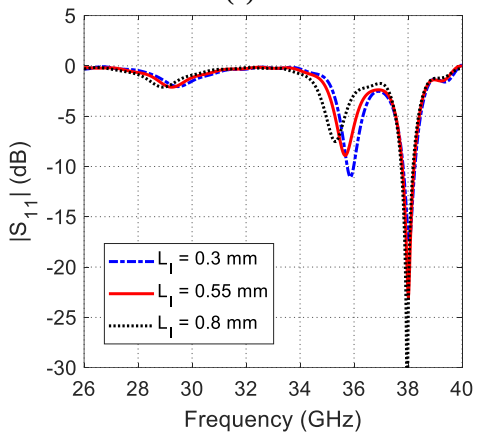

(b)

Fig. 6: Effect of changing the inset length, L_I, on the frequency response of $|S_{11}|$ for (a) $\Psi = 0°$ and (b) $\Psi = 90°$.

4. Simulation Results

This section is concerned with presenting the numerical results of the electromagnetic simulation obtained by the CST® simulator to investigate the performance of the reconfigurable dual-slot SIW antenna proposed in the present work.

4.1. Impedance Matching frequency Band

The magnitude of the reflection coefficient at the feeding port of the antenna, as obtained by simulation, varies over the frequency band 26-40 GHz as shown in Figure 7. For $\Psi = 0°$, the antenna for impedance is matched over the frequency band $27.6 - 28.7$ GHz with a minimum value of $|S_{11}| = -24$ dB exactly at 28 GHz. On the other hand, for$\Psi = 90°$, the antenna impedance is matched over the frequency band $37.5 - 38.4$ GHzwith a minimum value of $|S_{11}| = -23$ dB exactly at 38 GHz. Experimental verification of these results are performed and presented in Section 5.

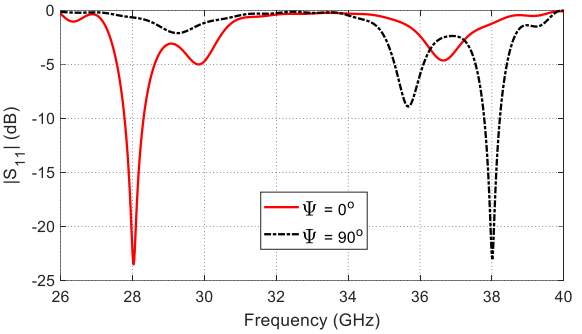

Fig 7: Frequency response of the reflection coefficient magnitude, $|S_{11}|$, at the antenna feeding port for $\Psi = 0°$ and $\Psi = 90°$.

4.2. Surface Current Distribution

The understanding of the current distribution on the surface of the radiating elements gives physical insight of the radiation mechanisms of the antenna at the operational frequencies. The current distributions on the surface of the upper wall of the cavity in the region around the slots are presented in Figures 8 and 9at 28 GHz (for $\Psi = 0°$) and 38 GHz (for $\Psi = 90°$), respectively. At 28 GHz, the surface current density is concentrated at the lower slot and showing 1^{st}-order pattern over the longer edge of the slot as shown in Figure 5. At 38 GHz, there are four radiating slots. In this case, the surface current density is concentrated at the upper two slots as shown in Figure 6. Owing to the smaller length of each slot, the current variation over its length exhibits 1^{st}-order pattern also. Thus, at the two frequencies, the radiation patterns will be similar as they are resulting from the same mechanism of radiation. A slight difference is that the radiation pattern resulting from two adjacent shorter slots (at 38 GHz) will be slightly narrower (resulting in slightly higher gain) than that resulting from a single longer slot (at 28 GHz).

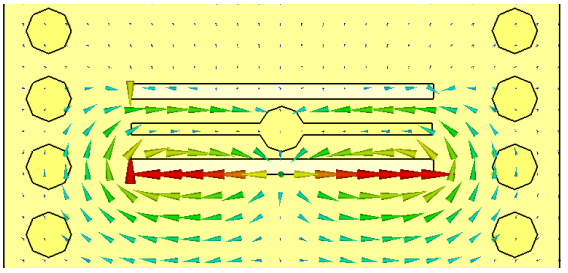

Figure 8: Surface current distribution when the antenna is configured to operate at 28 GHz, $\Psi = 0°$.

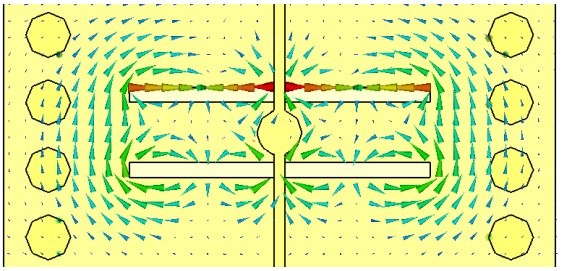

Figure 9: Surface current distribution when the antenna is configured to operate at 38 GHz, $\Psi = 90°$.

4.3. Radiation Patterns

The radiation patterns,obtained by simulation, for the proposed antennawhen configured to operate at28 and 38 GHz ,are presented in Figures10and 11, respectively. The radiation patterns are plotted in the elevation planes $\phi = 0°$ and $\phi = 90°$. It is shown that the radiation patterns in the elevation planes have balloon-likeshaped.This makes the antenna appropriate for operation as a single-element antenna as well as an element in array for beam forming. Also, the beam shapes in the elevation planes makes the antenna appropriate to be employed as an element in multiple-input-multiple-output (MIMO) antenna system for performance enhancement of the communication system. The values of the maximum gain obtained when the antenna is configured to radiate at 28 and 38 GHz are5.4dBi and 6 dBi, respectively. These results have been interpreted above (Section 4.2) in view of the current distribution on the antenna surface around the radiating slots. The radiation patterns are similar (with a slight increase in the gain at the higher frequency) because both of them are produced by 1st-order current distribution over the longer edges of the radiating slots. The gain at 38 GHz is produced by two adjacent slots and, hence, it is slightly higher than the gain at 28 GHz, which is produced by a single (but longer) slot.

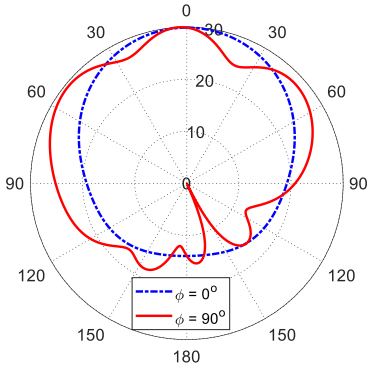

Figure 10: Radiation patterns at 28 GHz (for $\Psi = 0°$).

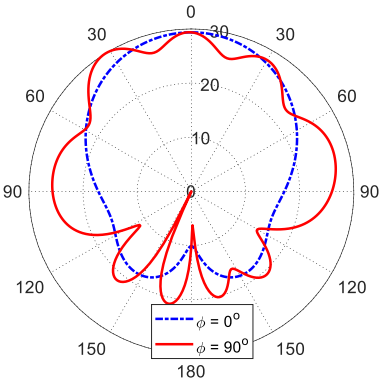

Figure 11: Radiation patterns at 38 GHz (for $\Psi = 90°$).

4.4. Maximum Gain

The variation of the maximum gain produced by the proposed reconfigurable dual-slot SIW antenna is presented in Figure 12. It is shown that the maximum gain obtained at 28 GHz for $\Psi = 0°$ is 5.4 dBi, whereas the maximum gain obtained at 38 GHz for $\Psi = 90°$ is 6 dBi. The slight difference of the gain is interpreted in view of the surface current distributions around the radiating slots as explained in Section 4.2.

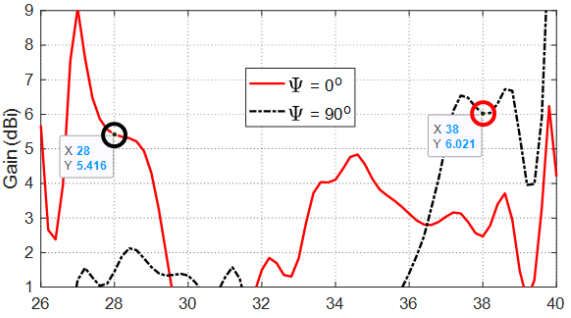

Fig.12: Variation of the maximum gain with the frequency when the antenna is configured to operate at 28 and 38 GHz, (i.e., when $\Psi = 0°$ and $\Psi = 90°$, respectively).

4.5. Antenna Efficiency

The radiation and total efficiencies of the reconfigurable SIW antenna vary with the frequency as shown in Figure 13 and 14 when the antenna is configured to operate at 28 and 38 GHz, respectively. The radiation efficiencies are 80.5% and 82% at 28 GHz and 38 GHz, respectively. The total efficiencies are 80% and 81.5% at 28 GHz and 38 GHz, respectively. The antenna efficiencies at 38 GHz are slightly higher than the efficiencies at 28 GHz because there are four radiating slots at 38 GHz whereas there are only two radiating slots at 28 GHz.

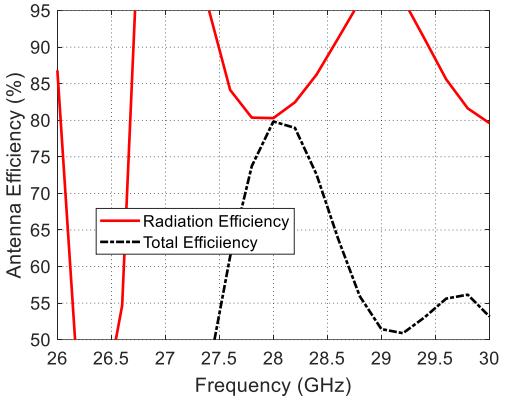

Figure 13: Variation of the radiation and total efficinecies of the reconfigurable SIW antenna when it is configured to operate at 28 GHz ($\Psi = 0°$).

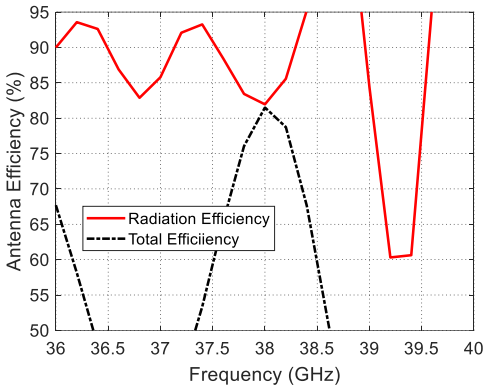

Figure 14: Variation of the radiation and total efficinecies of the reconfigurable SIW antenna when it is configured to operate at 38 GHz ($\Psi = 90°$).

5. Prototype Fabrication and Experimental Work

5.1. Prototype Fabrication

The proposed antenna with the dimensions listed in Tablet is fabricated by lithography on a substrate of the material Roger's R03003 ($\varepsilon_r = 3,\ \tan\delta = 0.001$) of thickness$h = 0.5$ mmrotary is added the. The rotary strip is placed on the external face of the upper wall of the SIW cavity with the axis of rotation at the center point of this wall. The rotary strip is allowed to be rotated within the angular range ($\Psi = 0°$ to $90°$) according to the required antenna configuration. Since the facilities required for fabricating the MEMS actuator are not currently available, the configuring strip is rotated manually about the center point, during measurement, in the same way as the rotation performed by the MEMS motor. This is quite enough to perform the required measurements. Finally, for being ready to measurement using the VNA model Key sight™ N5244B PNA-X, a coaxial launcher of type 1.85 mm is mounted at the feedingpoint of the microstrip line. A 1.85mm-male-to-1.0mm-female coaxial adaptor is used for connecting the antenna to the VNA cable. The fabricated prototype and the attached launcher and adaptor are shown in Figure 15.

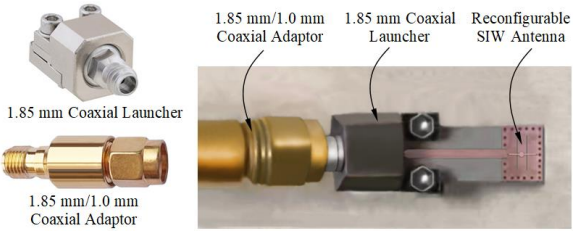

Fig.15: Fabricated prototype of the reconfigurable dual-slot SIW antenna. The 1.85 mm coaxial launcher is mounted to the antenna for measurements. A 1.85mm-male-to-1.0mm-female coaxial adaptor is used for connecting the antenna to the VNA cable.

5.2. Measurement of the Reflection Coefficient

The reflection coefficient at the port of excitation is measured when the antenna is configured to operate at 28GHz as well as 38 GHz using the VNA model Key sight™ N5244B PNA-X with its 110 GHz frequency extender. The corresponding results are presented in Figures 13 and 14, respectively. The measurements are compared to the simulation results and found to agree well with each other as shown in the figure.

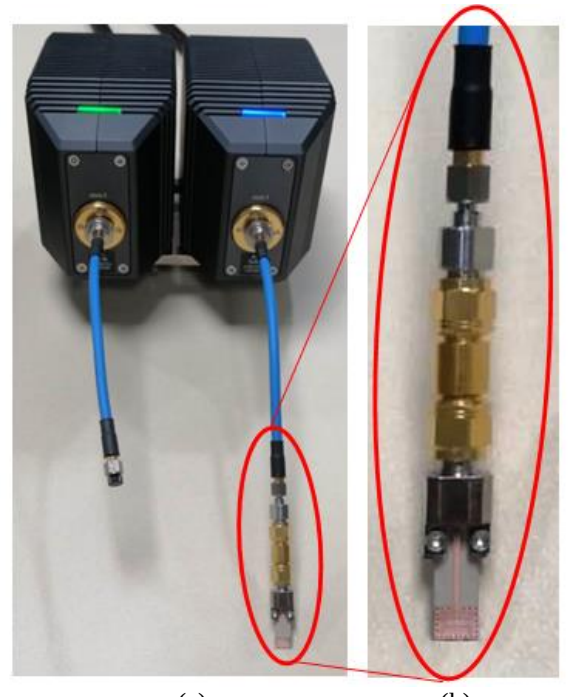

(a) (b)

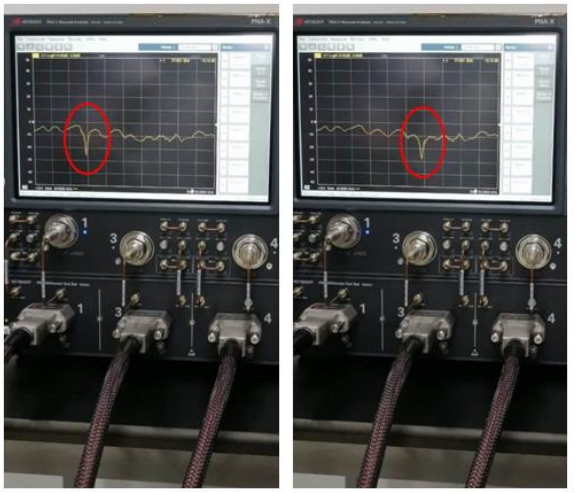

(c) (d)

Fig. 16: Measurement of the reflection coefficient, S_{11}, at the excitation port of the antenna by the VNA. (a) The antenna is connected to the frequency extender of the VNA model Keysight™N5244B PNA-X through a coaxial cable. (b) Zoomed view at the antenna. (c) Measured $|S_{11}|$ when the antenna is configured to operate at 28 GHz. (d) measured $|S_{11}|$ when the antenna is configured to operate at 28 GHz.

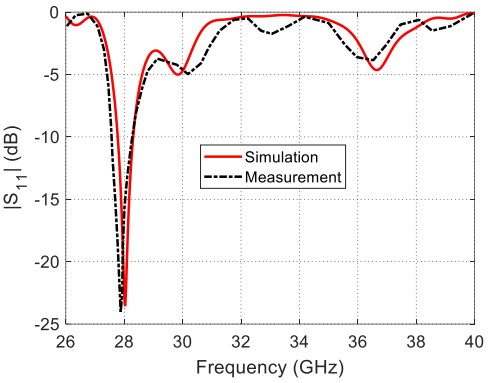

Figure 17: The measuered frequency response of $|S_{11}|$ when the reconfigurable SIW antenna is configured to operate at 28 GHz ($\Psi = 0°$). The measurements are compared to the simulation results.

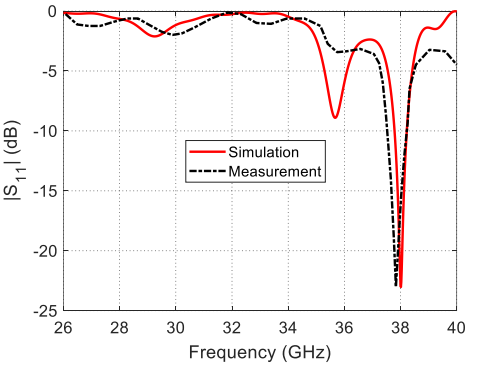

Figure 18: The measuered frequency response of $|S_{11}|$ when the reconfigurable SIW antenna is configured to operate at 38 GHz ($\Psi = 90°$). The measurements are compared to the simulation results.

6. Comparison with Other Related Antenna Designs

Some comparisons among reconfigurable the dimensions and performance of millimeter-wave antennas of different designs available in recent publications are listed in Table 2. It is shown that the antenna introduced in the present work is relative compact when compared with most of the listed antennas. It has reasonable bandwidth, gain, and efficiency. Moreover, the proposed antenna uses only one switching element whereas all the other antennas use two switching element.

Table 2: Comparison among reconfigurable millimeter-wave antennas of different designs available in recent publications

Work	Re-configurability	Switching	Dimensions mm×mm×mm	Frequency (GHz)	Bandwidth (GHz)	Gain (dBi)	Efficiency (%)
[1]	Frequency	2 PIN Diodes	43×32×0.63	25, 26, 27.75, 29	1.0	12	NA
[3]	Pattern	2 RF MEMS	3.7×5.2×0.4	35	0.85	5	NA
[12]	Frequency	2 PIN Diodes	30×7.5×0.25	28 38	1.0 0.4	7.2 10	94.0 88.0
[13]	Frequency	2 PIN Diodes	30×7.5×0.25	28 38	0.4 1.0	7.3 9.5	98.0 97.0
[14]	Frequency	2 RF MEMS	4.0×5.3×0.25	42.36, 47.65, 53.13, 56.72	1.0	7.9	NA
Present	Frequency	1 MEMS Actuator	7.4×5.6×0.5	28 38	1.1 0.9	5.4 6.0	80.5 82.0

7. Conclusion

A reconfigurable dual-slot SIW antenna has been proposed for future generations of mobile communication. The antenna has two parallel slots that are perpendicular to the axis of symmetry of the antenna and feeding line. The slots are cut in the upper wall of the SIW cavity. This antenna is reconfigurable and canoperate at either 28 or 38 GHz, where the frequency selection is performed by a rotary strip. This strip can be rotated touching the external surface of the upper wall of the SIW cavity by means of a MEMS actuator. When the rotary strip is rotated to be parallel to the slots it operates at 28 GHz. When the rotary strip is rotated to be perpendicular to the slots, the antenna operates at 38 GHz. In the latter case, each slot is divided into two slots to form four radiating slots of the same length. The proposed antenna has been fabricated and subjected to experimental investigations. The simulation and measurement agree well with each other and show high performance of the proposed antenna. The antenna has impedance matching bandwidths of 1.1GHz and 0.9 GHz about the centre frequencies 28 and 38 GHz, respectively. The maximum gain obtained at 28 GHz is 5.4 dBi, whereas the maximum gain obtained at 38 GHz is 6 dBi. The radiation efficiencies of the proposed antenna are 80.5% and 82% at 28 GHz and 38 GHz, respectively. The total efficiencies are 80% and 81.5% at 28 GHz and 38 GHz, respectively.

References

[1] Deng, Zhongliang, Yucheng W., and Chengqi L., "Design and Analysis of Pattern Reconfigurable Antenna Based on RF MEMS Switches", Electronics 12, no. 14, 3109, 2023.

[2] Cano, Pablo Z., Zaharias D. Z., Traianos V. Y., Nikolaos V. K., and Pavlos I. L., "Pattern reconfigurable antennas at millimeter-wave frequencies: A comprehensive survey", IEEE Access 10, 83029-83042, 2022.

[3] Antunes, Filipa, Amélia R., Tiago V., and João N. M., "Concept and Design of a Multi-Polarization Reconfigurable Microstrip Antenna with Symmetrical Biasing Control" ,Sensors 24, no. 8, 2408, 2024.

[4] Wang, Shenyun, Danping Y., Wen G., Chen Z., and Guowen D., "Polarization-reconfigurable antenna using combination of circular polarized modes", IEEE Access 9, 45622-45631, 2021.

[5] Sathuluri, Mallikharjuna R., and Sasikala,"Reconfigurable antenna using RF MEMS switches issues and challenges: A survey", Advances in Smart System Technologies: Select Proceedings of ICFSST 2019, 119-134, 2021.

[6] Quddious, Abdul, Muhammad A. B. A., Marco A. A., Photos V., Vincent F., and Symeon N.,"Dynamically reconfigurable UWB antenna using an FET switch powered by wireless RF harvested energy", IEEE Transactions on Antennas and Propagation 68, no. 8, 5872-5881, 2020.

[7] Du, Yuxuan, Yan W., Yuefei Y., Weixing Y., Pengying X., Xiaoxian X., Dengfeng W., Nianke Z., Meng W., and Congsi W., "Reconfigurability enhancement of pixel array antennas based on WOA and MPUC", AEU-International Journal of Electronics and Communications 178, 155240, 2024.

[8] Qin, Jiamei, Xuedong F., Mingyu S., Qiang R., and Aixin C., "Frequency reconfigurable antenna based on substrate integrated waveguide for S-band and C-band applications", IEEE Access 9, 2839-2845, 2020.

[9] Goel, Shivam, and Navneet G., "Design, optimization and analysis of reconfigurable antenna using RF MEMS switch", Microsystem Technologies 26, no. 9, 2829-2837, 2020.

[10] Balarajuswamy, and Nakkeeran R., "Reconfigurable SIW antenna at 28/38 GHz for 5G applications", International Journal on Interactive Design and Manufacturing (IJIDeM) 17, no. 6, 2977-2986, 2023.

[11] Balarajuswamy, and Nakkeeran R., "Efficiency enhancement of reconfigurable SIW antenna for millimeter-wave applications", Wireless Personal Communications 127, no. 4, 2727-2742, 2022.

[12] Chen, Yu, Honglei G., Yanfei L., Jing L., Yongxin Z., Qiannan W., and Mengwei L., "An L-Slot Frequency Reconfigurable Antenna Based on MEMS Technology", Micromachines 14, no. 10, 1945, 2023.

[13] Patriotis, Marios, Firas N. A., Youssef T., Joseph C., and Christos G. C.,"A millimeter-wave frequency reconfigurable circularly polarized antenna array", IEEE Open Journal of Antennas and Propagation 2, 759-766, 2021.

[14] AL-fadhali, Najib, Huda A. M., Rosli O., Jumadi A.S., Mohamad K.R., Zuhairiah Z.A., Mohammed Al-B., Abdul M. M., and Najmaddin A.M., "Review on frequency reconfigurable antenna using substrate-integrated waveguide for cognitive radio application", Journal of Electromagnetic Waves and Applications 35, no. 7, 958-990, 2021.

[15] Tai Y.C., Fan L.S., and Richard S. M., "IC-processed micro-motors: Design, technology, and testing", In IEEE Micro Electro Mechanical Systems, Proceedings, 'An Investigation of Micro Structures, Sensors, Actuators, Machines and Robots, IEEE, pp. 1-6, 1989.

[16] Fan L.S., Tai Y.C., and Richard S. M., "Integrated movable micromechanical structures for sensors and actuators", IEEE Transactions on Electron Devices 35, no. 6, 724-730, 1988.

[17] Williams, and Le H. R., "Tribology and MEMS", Journal of Physics D: Applied Physics 39, no. 12, 2006.